

# Ground Structures-Based Topology Optimization of a Morphing Wing Using a Metaheuristic Algorithm

Seksan Winyangkul <sup>1</sup>, Kittinan Wansaseub <sup>1</sup>, Suwin Slesongsom <sup>2</sup> , Natee Panagant <sup>1</sup> , Sumit Kumar <sup>3</sup> , Sujin Bureerat <sup>1</sup>  and Nantiwat Pholdee <sup>1,\*</sup> 

<sup>1</sup> Sustainable and Infrastructure Development Center, Department of Mechanical Engineering, Faculty of Engineering, Khon Kaen University, Khon Kaen City 40002, Thailand; seksanwin@kkumail.com (S.W.); kittinan\_w@kkumail.com (K.W.); natapa@kku.ac.th (N.P.); sujbur@kku.ac.th (S.B.)

<sup>2</sup> Department of Aeronautical Engineering, International Academy of Aviation Industry, King Mongkut's Institute of Technology Ladkrabang, Bangkok 10520, Thailand; suwin.se@kmitl.ac.th

<sup>3</sup> Australian Maritime College, College of Science and Engineering, University of Tasmania, Launceston 7248, Australia; sumit21sep1990@gmail.com

\* Correspondence: nantiwat@kku.ac.th; Tel.: +66-043-362145-6

**Abstract:** This paper presents multi-objective topology and sizing optimization of a morphing wing structure. The purpose of this paper is to design a new aircraft wing structure with a tapered shape for ribs, spars, and skins including a torsion beam for external actuating torques, which is anticipated to modify the aeroelastic characteristic of the aircraft wing using multi-objective optimization. Two multi-objective topology optimization problems are proposed employing ground element structures with high- and low-grid resolutions. The design problem is to minimize mass, maximize difference of lift effectiveness, and maximize the buckling factor of an aircraft wing subject to aeroelastic and structural constraints including lift effectiveness, critical speed, and buckling factors. The design variables include aircraft wing structure dimensions and thickness distribution. The proposed optimization problems are solved by an efficient multi-objective metaheuristic algorithm while the results are compared and discussed. The Pareto optimal fronts obtained for all tests were compared based on a hypervolume metric. The objective function values for Case I and Case II at 10 selected optimal solutions exhibit a range of structural mass as 115.3216–411.6250 kg, 125.0137–440.5869 kg, lift effectiveness as 1.0514–1.1451, 1.0834–1.1639 and bucking factor as 38.895–1133.1864 Hz, 158.1264–1844.4355 Hz, respectively. The best results reveal unconventional aircraft wing structures that can be manufactured using additive manufacturing. This research is expected to serve as a foundation for future research into multi-objective topology optimization of morphing wing structures based on the ground element framework.

**Keywords:** aeroelasticity; aircraft wing; internal wing structure; multi-objective evolutionary algorithms; metaheuristics



**Citation:** Winyangkul, S.; Wansaseub, K.; Slesongsom, S.; Panagant, N.; Kumar, S.; Bureerat, S.; Pholdee, N. Ground Structures-Based Topology Optimization of a Morphing Wing Using a Metaheuristic Algorithm. *Metals* **2021**, *11*, 1311. <https://doi.org/10.3390/met11081311>

Academic Editors: José Valdemar Fernandes and Paolo Ferro

Received: 30 June 2021

Accepted: 17 August 2021

Published: 19 August 2021

**Publisher's Note:** MDPI stays neutral with regard to jurisdictional claims in published maps and institutional affiliations.



**Copyright:** © 2021 by the authors. Licensee MDPI, Basel, Switzerland. This article is an open access article distributed under the terms and conditions of the Creative Commons Attribution (CC BY) license (<https://creativecommons.org/licenses/by/4.0/>).

## 1. Introduction

Weight reduction in conjunction with increased structural and aero-elastic performances such as flutter speed, buckling is vital for competitiveness in the aircraft industry. Therefore, the design and development process of aircraft is essential to boost the potential of aircraft wing structures. However, with conventional wing design standards that pose limitations of fixed structure and control surfaces, it is very difficult to achieve maximum performance.

Hence, to reach the highest performance of the aircraft over the flight envelope, the notion of morphing aircraft is becoming interesting for researchers. This is because adjusting aircraft structures can improve flying performance, control authority, fuel consumption, and multi-mission capabilities to some extent [1,2]. However, due to the limitation of cost

and manufacturing technology, a morphing aircraft apprehension is not popular for real use previously. Nowadays, several new manufacturing technologies have been developed such as 3D printing and additive manufacturing (AM), which can improve the capability of manufacturing and make the impossible possible. Therefore, manufacturing a morphing frame has a higher possibility and design optimization of morphing wings is an interesting topic.

The hypothesis of morphing wings can be classified into three main categories: planform morphing, plane morphing, and airfoiled morphing [3]. The planform morphing adjusts the wing structure by changing the wingspan, chord, and sweep [4] while the plane morphing wing adjusts its structure by changing twist, dihedral/gull, and span-wise bending [5,6]. For the airfoiled morphing concept, the wing structure is adjustable by changing the camber and thickness-to-chord [7]. Based on these three morphing types, the performance of the aircraft can be improved in several dimensions. For example, adjusting wingspan, chord, and sweep in the planform morphing leads to the benefit of small and large flight endurance in aircraft, flight performance, roll control, flutter suppression, lift, and longitudinal stability [8]. Albeit adjusting twist distribution dihedral/gull, and span-wise bending of the plane morphing generates the benefit of flight performance, control authority, reducing of drag, increasing stall characteristic, and enhancing agility and maneuverability [9]. Moreover, adjusting camber morphing and thickness-to-chord morphing is favorable for high lift generation and drag curtailment. The camber changing can be used for roll, pitch, and yaw control [10].

Formerly, topology optimization (TO) has been used to redesign the aero-structure components in commercial aircraft components [11,12], which has the main expectation to make it safer and lighter. One of the redesign components is a morphing aircraft wing. The recent development in aero-structure designs is a successor of the previous studies in the field of TO. The process of aircraft structural optimization can be separated into three stages viz. topology, sizing, and shape optimization [13]. The combination of topological and sizing stages in the design of aircraft wing structures is also popular compared to shape optimization [14–16]. The combination included the ground structure method or a discrete design variables approach. This method is called partial TO, which can find a structural layout and dimensions at the same time [15,17]. The ground structure approach has been proposed to improve the traditional spectrum of TO (the approach based on material density) [18], which is expected to avoid unrealizable design results. In general, the design domain is discretized as trusses, frames, and panels. By varying the pseudo-density of each member between zero (voids) and one (presence of material), the structural layout and component sizes in the design domain can be defined in one optimization run. This framework has been applied for synthesizing adaptive trailing edge structures [19]. The work is attracted by many researchers to develop concepts of adaptive or morphing wings [20,21]. The wing can improve aircraft performances in flight by shape-changing to alleviate aeroelastic phenomena such as divergence and flutter speed. Previously, the TO problem based on material density distribution has been used to synthesize ribs [11,12,22,23], spars [23,24], stiffened panels [25], and the whole of aircraft wing [26,27]. Later, the results from TO have been fulfilled with AM technology, which reached the success of the development of morphing aircraft wing structures [28] and the movable rudder [29]. The first work proposed a composite AM of morphing wing drone while the second work presented a movable rudder design by thermo-elastic TO and AM. Although the success presents the performance of the AM to manufacture, the complex morphing structures designed by the TO framework are still a problem. The efficiency of AM can be deviated due to the loss of geometric accuracy and performance deterioration when the TO is performed with the material density method [30]. The ground structure method can result in structural layout and sizing of the aircraft wing structure in one optimization run, which is a choice for generating unconventional aircraft wing structure [20,21,26]. Therefore, the design results are proved that these peculiar

structures can be used in practice. The unconventional structural design looks possible for manufacturing [22] while it has repeatability to produce [30].

As mentioned above, the key of the morphing wings is the internal structure which can be classified as a compliant mechanism [17,20,21]. The internal structure of morphing wings needs to be optimized to meet the best possible wing performance while the optimization problem can be both single and multi-objective (MO) to minimize the structural mass and/or maximizing aircraft tall flight performance subjected to several constraints such as flutter speed, flexibility, buckling factor, etc., [31]. The topology and size of the structure are the most popular design variables considered so far in the literature. Over the past decade, the TO of morphing wings has been successfully presented based on both concepts of ground structures [17] and ground elements [20] topology.

Optimization techniques based on metaheuristic or evolutionary algorithms, on the other hand, have also been successfully applied for both single-objective [32,33] and MO problems [34,35]. Although numerous investigations on TO of morphing wings have been studied, most of the work focuses on investigating the performance of an aeroelasticity analysis tool, an optimization solver tool, and an optimum structure. It was found in the literature that there is rarely a work-study on the effect of the resolution of the ground structure or ground element on the design results and computational time.

Therefore, this work concentrates on this research gap, aiming to investigate the effect of ground structure topology resolution on wing morphology while also presenting a novel design for a morphed wing structure. The innovative morphed wings investigated employ a torsion beam for actuating and skeletal elements as internal structure instead of conventional wing ribs and inside spars as shown in Figure 1. The optimization problem is posed to minimize wings mass, maximize difference of lift effectiveness, and maximize buckling factor subjected to aeroelastic and structural constraints including lift effectiveness, critical speed, and buckling factors. The design variables are thickness for ribs, spars, and skins, distribution thickness function decision, and topology and sizes of skeletal elements. Two MO problems are proposed based on skeletal ground structures with high- and low-grid resolutions. The proposed optimization problems are solved by multi-objective metaheuristic with iterative parameter distribution estimation (MM-IPDE) while the results obtained from the skeletal ground element structures with high- and low-grid resolutions are compared and discussed. The remaining of this paper is divided into five sections. Section 2 shows the details of the aircraft wing model and its aeroelastic analysis while the details of the experimental setup are presented in Section 3. The results and discussion, and conclusions are detailed in Sections 4 and 5, respectively.

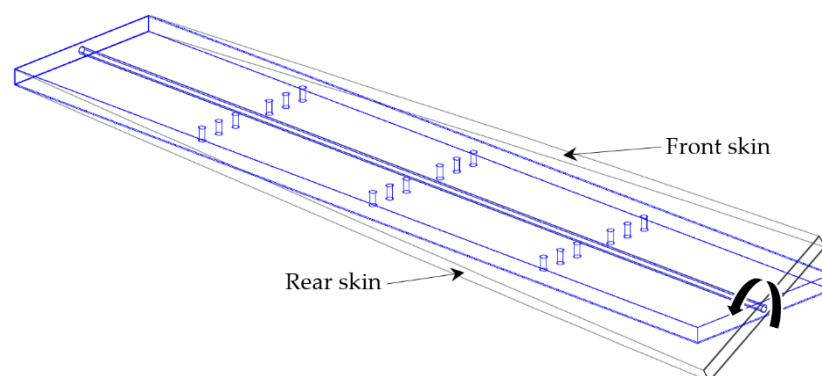


**Figure 1.** New concept morphing wings presented torsion beam.

## 2. Aircraft Wing Model

In this work, a new concept of morphing wing structure is proposed via employing skeletal elements as part of the internal structure instead of conventional wing rib and spar while the actuator is modelled as a torsion beam. The Golland wing is a rectangular-shaped frame that is comprised of leading, trailing, and center edge spar including 11 ribs as shown

in Figure 2a. It is selected for the present case study and is modelled as an Aluminum wing box (7075 Aluminum alloy) while the material properties of the wing are shown in Table 1. The chord length and semi-span of the wing are 1.216 m and 6.096 m., respectively while the wing thickness is 0.0508 m. The comparison of the internal wing structure of the original Golang wing and the proposed internal concept structure are shown the Figure 2.

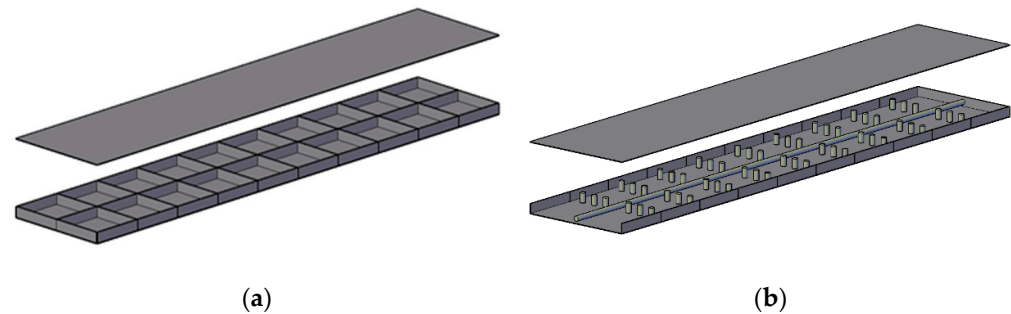


**Figure 2.** Golang wings (a) original Golang wing structures (b) a new concept of aircraft wing structures.

**Table 1.** Material properties of aluminum.

Properties	Value	Unit
Young's modulus (E)	$70 \times 10^9$	Pa
Poisson's ratio ( $\nu$ )	0.3	-
Density ( $\rho$ )	2700	kg/m <sup>3</sup>

### 2.1. Aerodynamic Model

In this paper, a quasi-steady vortex ring method [17] is used for aerodynamic analysis. The aerodynamic forces acting on the structure can be represented as follows:

$$f(t) = q[G]^T[S][AIC(k)][G]^T\{u\} \quad (1)$$

where  $k = \frac{L\omega}{V}$  is the reduced frequency,  $L$  is a semi chord length,  $V$  is wind velocity,  $\omega$  is a circulation frequency,  $q$  is dynamic pressure,  $[S]$  is the diagonal matrix of panel areas,  $[AIC]$  is the aerodynamic influence coefficient matrix,  $[G]$  is the transformation matrix, and  $\{u\}$  is a vector of structural displacements of the wing finite element model. It should be noted that more accurate aeroelastic analysis can be obtained by using the unsteady aerodynamic analysis such as the doublet lattice method, however, it has been shown in our previous study that the quasi-steady vortex ring method gives acceptable results.

### 2.2. Aeroelasticity Analysis

The wing aeroelasticity model considered herein is established by the mutual interaction of three forces i.e., inertial, elastic, and aerodynamic forces. The governing equation can be written as:

$$[M]\{\ddot{u}\} + [D]\{\dot{u}\} + [K]\{u\} = [A_d(V)]\{\dot{u}\} + [A_k(V)]\{u\} \quad (2)$$

where  $[M]$ ,  $[D]$ ,  $[K]$  depicts the mass, damping, and stiffness matrices of the wing structure.  $[A_d]$  and  $[A_k]$  are aerodynamic damping and stiffness matrices respectively. The latter two matrices are the cause of fluid/structure interaction, which will modify the system damping and stiffness while they are dependent on velocity.

### 2.3. Flutter Analysis

The flutter speed is a speed at which the dynamic system becomes unstable. Such a speed can be determined by sweeping the value of wind velocity  $V$  from lower to higher. With a given wind speed, a state-space matrix can be formed while the real parts of its

eigenvalues are negative if the wing aeroelastic system is stable. The flutter speed is found when one of the real parts of the eigenvalues is zero.

#### 2.4. Divergence Analysis

The divergence is usually represented as a speed when the aerodynamic load overcomes the structural restoration, considered at the steady-state condition. The governing equation can be obtained from Equation (2) by removing the terms related to time written as

$$[K]\{u\} = q[A_k]\{u\} \quad (3)$$

The system leads to an eigenvalue problem. Since the aerodynamic stiffness matrix can be singular, it is more useful to modify the problem as

$$\left([K]^{-1}[A_k] - \lambda[I]\right)\{u\} = \{0\} \quad (4)$$

where  $\lambda = \frac{1}{q}$ . Once the eigenvalue problem (4) is solved, the largest value of  $\lambda$  will give the lowest divergence speed.

#### 2.5. Lift Effectiveness

The lift effectiveness is defined as the ratio of lift force on the flexible structure to its rigid counterpart, therefore, can be computed as:

$$\eta_L = \frac{qS^T[AIC]_F\alpha}{qS^T[AIC]_R\alpha} \quad (5)$$

where  $q = \frac{1}{2}\rho_{air}V^2$  is the dynamic pressure,  $\rho_{air}$  is the air density,  $S$  is the matrix of panel areas, and  $\alpha$  is the vector of the panels' angles of attack.  $[AIC]_F$  is the flexible surface aerodynamic influence coefficient matrix. It is alternatively called the ratio of cruise shape lift to jig shape lift.

#### 2.6. Buckling Analyses

Buckling due to aerodynamic loads is crucial for aircraft wing design as most parts of the wing are plate-like. In this work, linear buckling analysis is employed. The buckling phenomenon takes place when the work done by in-plane stress due to bending displacement on the wing overcomes its elastic potential energy. Such a situation leads to an eigenvalue problem.

$$[K]\{u\} - \lambda[K_G] = \{0\} \quad (6)$$

where  $\lambda$  is a buckling factor,  $[K]$  depicts the structural stiffness matrix, and  $[K_G]$  illustrates a global geometrical matrix.

### 3. Numerical Experiment

#### 3.1. The Proposed Multiobjective Ground Structure Topology Optimization Problem

Two cases of MO ground structure TO design problem of the newly proposed concept of Goland wing are presented based on low (Case I) and high (Case II) grid resolutions. Moreover, 18 and 54 pieces of skeletal rods distributed in the wing internal structure are considered to be a ground structure for Case I and Case II respectively as demonstrated in Figures 3 and 4.

The MO optimization problem is posed to minimize structural mass, maximize buckling factor, and maximize the difference of lift effectiveness due to counterclockwise and clockwise twists of the beam subject to aeroelasticity constraints while the design variables are sizing of ribs, spars, skins and torsion beam, distribution thickness function decision, topology, and sizing of the skeletal rods as presented in Figure 3. The first objective function is set to have a low inertia structure while the second objective is set to enhance the structural static stability. The third objective is the difference between the wing lift effective-

ness due to counterclockwise and clockwise twist on the beam. This indicator determines the ability to control lift force on the wing through control actuation from twisting the beam. Thus, this wing works with the concept of morphing wing. The investigated MO optimization problem can be expressed as follows:

$$\text{Min}_x f_1(x) = \text{total mass}, \text{Max}_x f_2(x) = \lambda, \text{Max}_x f_3(x) = \Delta\eta_L \tag{7}$$

subject to

$$V_{f,al} - V_f \leq 0 \tag{8}$$

$$\eta_{L,al,max} - \eta_L \leq 0 \tag{9}$$

$$\eta_L - \eta_{L,al,max} \leq 0 \tag{10}$$

$$\lambda_{al} - \lambda \leq 0 \tag{11}$$

$$x_4 - x_3 \leq 0 \tag{12}$$

$$x_7 - x_6 \leq 0 \tag{13}$$

$$x_{10} - x_9 \leq 0 \tag{14}$$

$$x_{13} - x_{12} \leq 0 \tag{15}$$

$$x_{16} - x_{15} \leq 0 \tag{16}$$

$$x_l \leq x \leq x_u$$

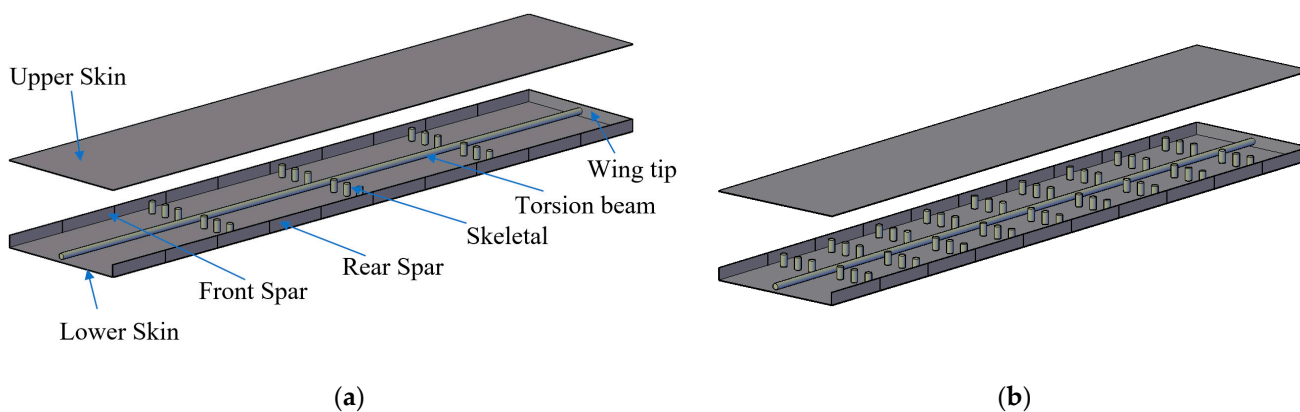


Figure 3. Goland wing modifications in (a) Case. I and (b) Case. II.

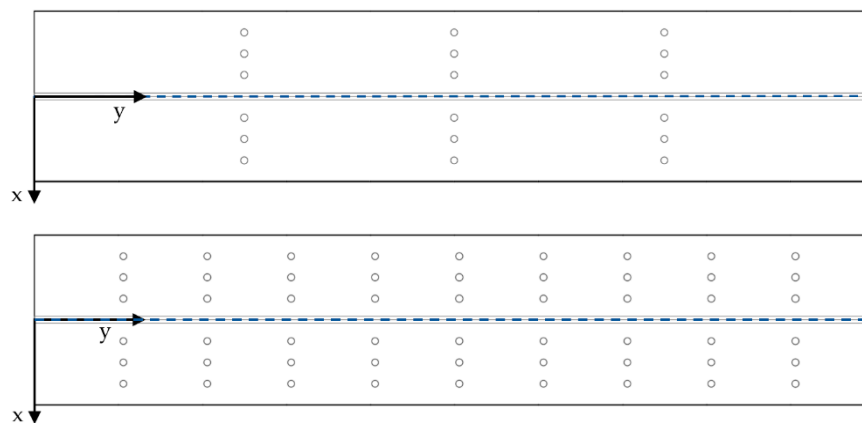


Figure 4. Skeletal rods positions in x-y plan for Goland wing modifications in Case. I and Case. II.

The above expression includes numerous variables where  $x$  is a vector of design variables having lower and upper bounds as  $x_l$  and  $x_u$  followed by

$\eta_L$  is the wing lift effectiveness.

$\eta_{L,al,min}$  is the minimum allowable value of lift effectiveness.

$\eta_{L,al,max}$  is the maximum allowable value of lift effectiveness.

$V_f$  is a critical wind speed herein is a flutter speed.

$V_{f,al}$  is an allowable value of critical wind speed.

$\lambda_{al}$  is the permissible magnitude of buckling factor.

$\lambda$  is the minimum magnitude of buckling factor.

$x_1$  is the diameter of the torsion beam.

$x_2$  is the distribution thickness function of the root front spar.

$x_3$  is the thickness of the root front spar.

$x_4$  is the thickness of the tip front spar.

$x_5$  is the distribution thickness function of the root rear spar.

$x_6$  is the thickness of the root rear spar.

$x_7$  is the thickness of the tip rear spar.

$x_8$  is the distribution function of ribs.

$x_9$  is the thickness of leading tip ribs.

$x_{10}$  is the thickness of trailing tip ribs.

$x_{11}$  is the distribution thickness function of lower skin.

$x_{12}$  is the thickness of root lower skin.

$x_{13}$  is the thickness of tip lower skin.

$x_{14}$  is the distribution thickness function of upper skin.

$x_{15}$  is the thickness of root upper skin.

$x_{16}$  is the thickness of tip upper skin.

$x_{17-34}$  is the diameter of skeletal rods(for only Case I).

$x_{17-70}$  is the diameter of skeletal rods(for only Case II).

The minimum and maximum allowable values of lift effectiveness are set to be  $\eta_{L,al,min} = 0.9$ ,  $\eta_{L,al,max} = 1.2$  and allowable value of the critical wind speed is at  $V_{f,al} = 100$  m/s. The design variable vectors are defined as a discrete value where the constraints are as follows.

$\{x_1, x_3, x_4, x_6, x_7, x_9, x_{10}, x_{12}, x_{13}, x_{15}, x_{16}\} \in \{0.5, 0.7, 0.8, 1.0, 1.2, 1.5, 2.0, 2.5, 3.0, 4.0, 5.0, 6.0, 8.0, 10.0, 12.0, 15.0, 16.0, 20.0, 25.0, 30.0, 35.0, 40.0, 45.0, 50.0\}$  mm.

While  $x_{17-34}$  (for Case I) or  $x_{17-70}$  (for Case II) are chosen from

$\{x_{17-34}, x_{17-70}\} \in \{0, 1.0, 1.2, 1.5, 2.0, 2.5, 3.0, 4.0, 5.0, 6.0, 8.0, 10.0, 12.0, 15.0, 16.0, 20.0, 25.0, 30.0, 35.0, 40.0, 45.0\}$  mm.

Note that when the decision variable for beam diameter is equal to zero it means that it will be deleted leading to the variation of wing topology. For the elements of  $\{x_2, x_5, x_8, x_{11}, x_{14}\}$  as decision variables for thickness distribution values, one of the six distribution functions cases (as shown in Figure 5) is selected.

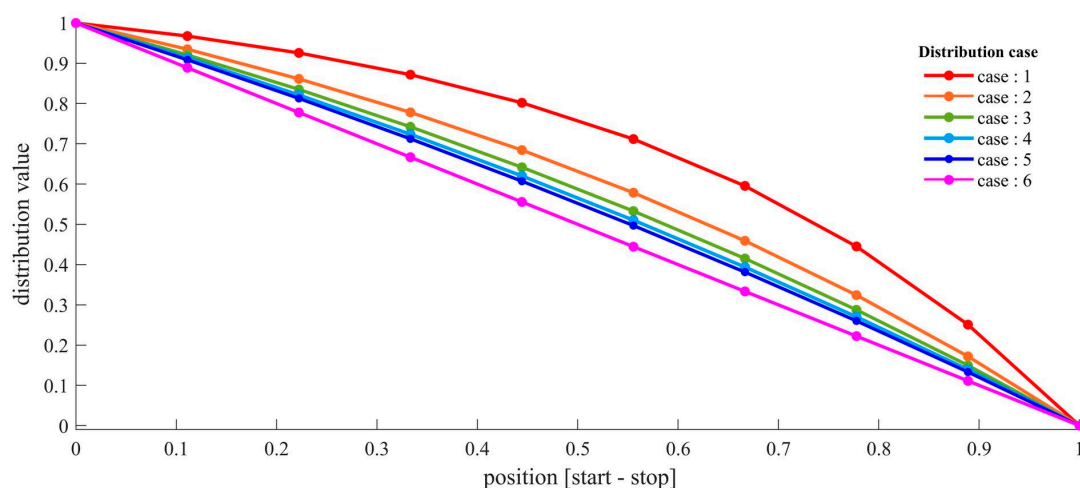
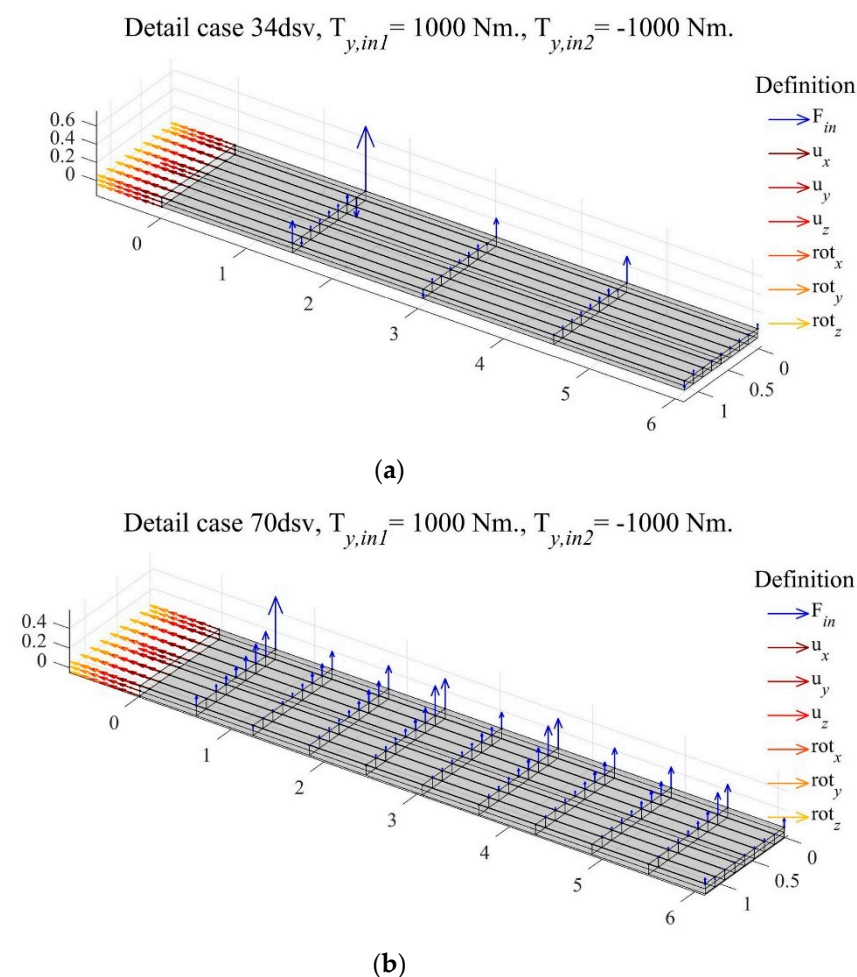


Figure 5. Distribution functions for determining the thickness of taper wing skins, ribs, and spars.

### 3.2. Numerical Simulation Model

The new design concept of the aircraft wing structure is demonstrated using the combination of MATLAB R2016b and ANSYS 2020 R2 Student Version software. The optimization process consists of running the MM-IPDE algorithm while function evaluations are achieved using finite element analysis (FEA) for static, buckling, and modal analyses. Aerodynamic loads are computed using the vortex ring method (equivalent to the vortex lattice method) as MATLAB codes. During the flight, the wing is subject to static aerodynamic loads at cruise speed, which means the stress and buckling constraints due to such applied loads are taken into consideration. The static aeroelastic phenomena, divergence speed, and lift effectiveness are computed in MATLAB by extracting a structural global stiffness matrix from ANSYS. Meanwhile, flutter analysis is carried out using a quasi-steady approach meaning that the effect of unsteady aerodynamic is excluded. It should be noted that this work is an initial study. If the more realistic wing is to be synthesized, the more accurate unsteady aerodynamic such as the doublet lattice method should be employed. For FEA with ANSYS, the shell element SHELL181 is used for wing skins, tip chord, and spars whereas all of the skeletal parts are modelled with the three-node line element BEAM188. The element size for automatic meshing is set to be 0.5 mm. Material properties of the aluminum alloy materials are those embedded in the ANSYS Library. The boundary condition set for the wing structure simulation is shown in Figure 6. A  $\pm 1000$  N-m torque is applied at the right end surface of the torsion beam while the left end of the wing surface is kept fixed. Aerodynamic force calculated based on the air density ( $\rho_{air} = 1.2 \text{ kg/m}^3$ ) and free stream velocity ( $=40 \text{ m/s}$ ) are applied over the wing surface.



**Figure 6.** Boundary condition set for the wing structure simulation in (a) Case. I. and (b) Case. II.

The optimization procedure is illustrated in Figure 7. Herein the two proposed MOTO cases are solved by the MM-IPDE technique. The population size is set to be 50 while the number of iterations is set to be 200. The computing times for Case I, Case II are 82.4976 and 153.2991 h, respectively.

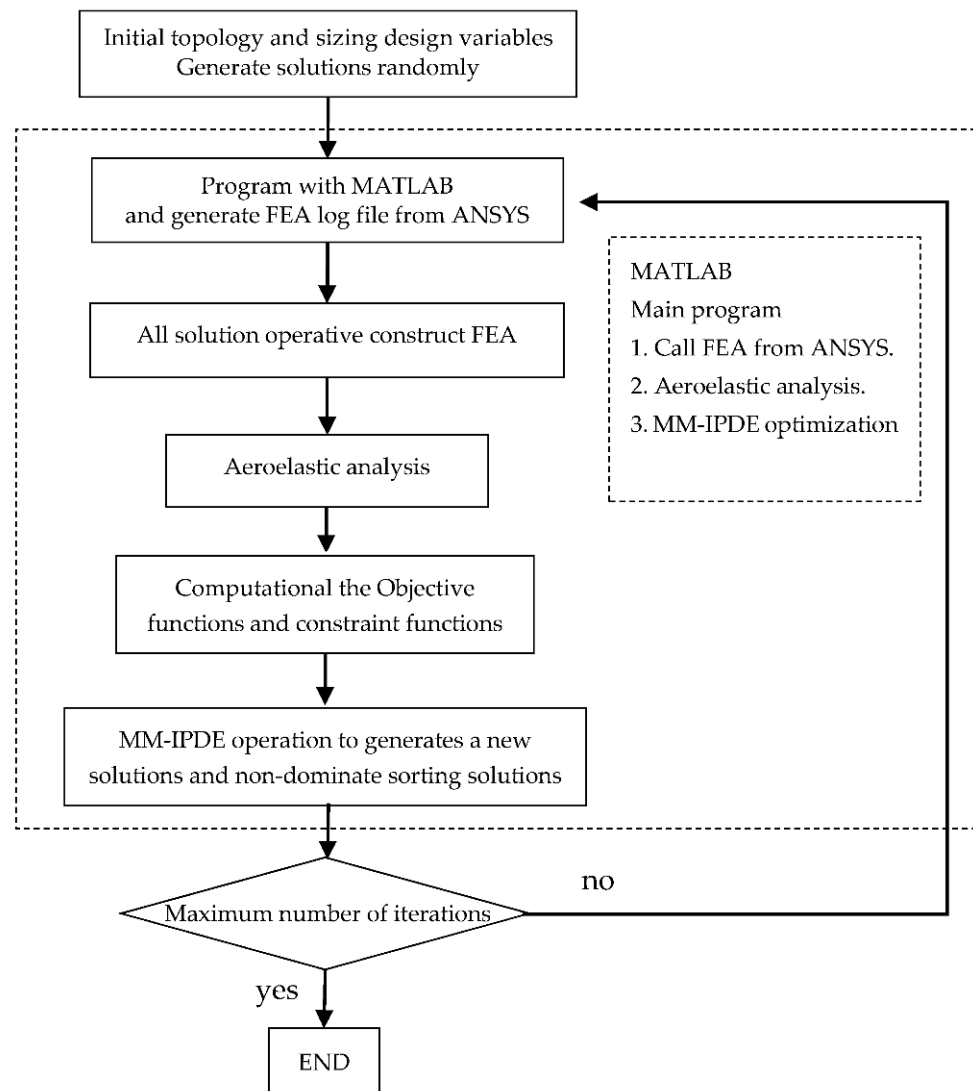
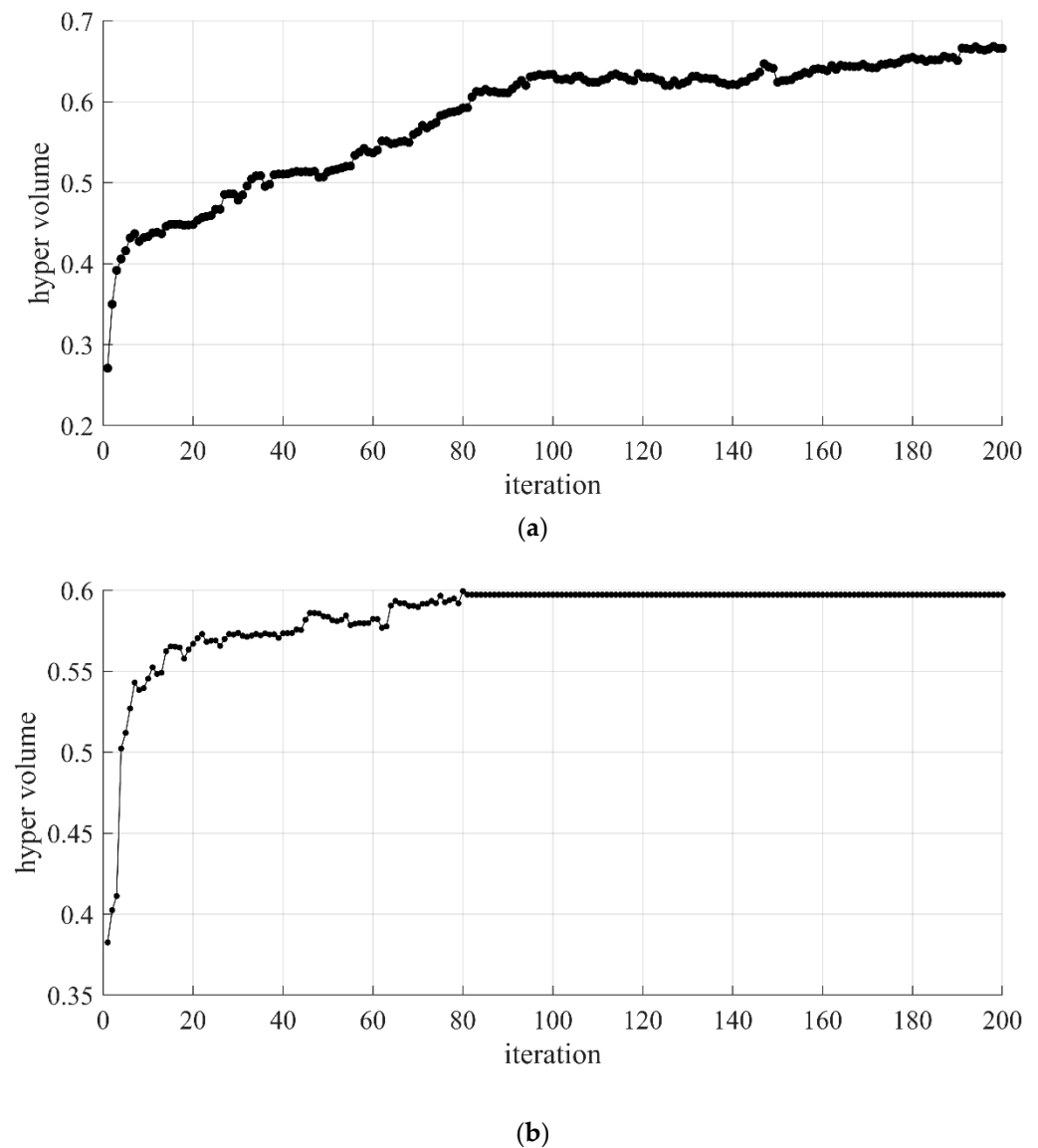


Figure 7. The process of a MOTO simulation model.

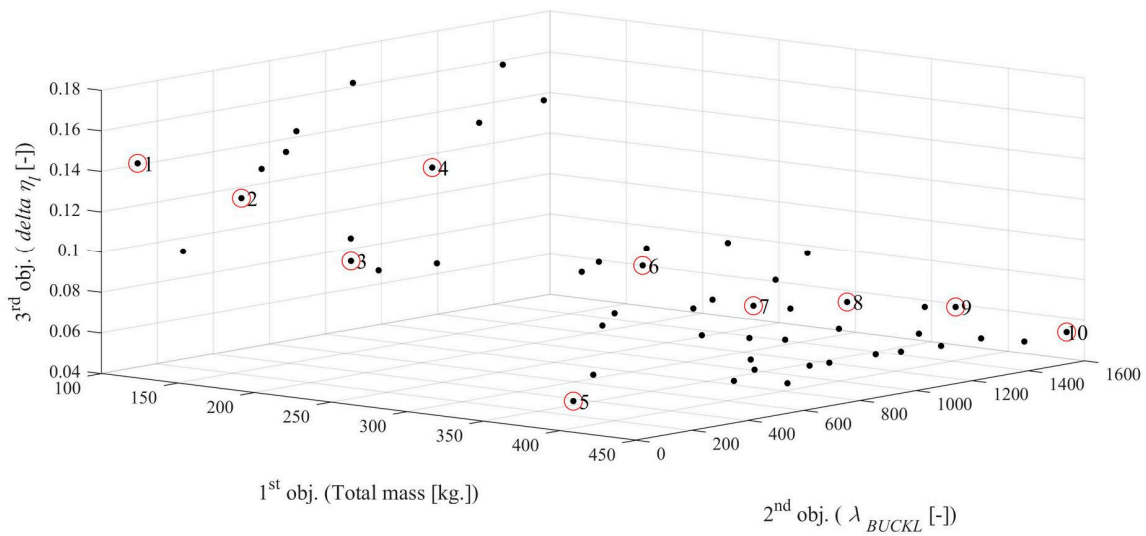
#### 4. Result and Discussion

The new aircraft wing structural optimization solves the problem using a computer with the following specification: AMD Ryzen 7 3700X with Radeon Graphics 3.00 GHz, 32.00 GB, 64-bit Window 10 operating system. Having performed the optimization runs of the proposed MOTO challenge based on the MM-IPDE, the hypervolume indicator is used to measure the quality of the Pareto front. Figure 8 shows the search history based on the hypervolume values for both cases of low (Figure 8a) and high (Figure 8b) grid resolutions. The figure indicates that the results converged after 100 and 80 iterations for the design Case I and Case II respectively. This implies that the problem with a higher number of design variables or high resolution of ground structure has a faster convergence rate.

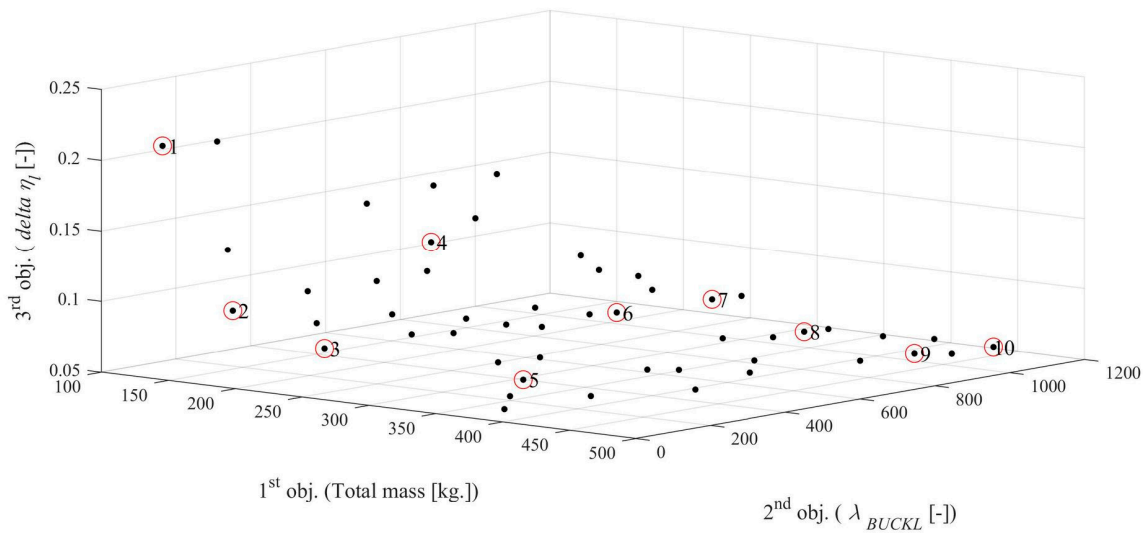


**Figure 8.** Hypervolume history for the convergence rate of the optimizers in (a) Case. I. and (b) Case. II.

Figure 9 shows the Pareto optimal fronts obtained from Case I and Case II while the objective function values of 10 selected optimal solutions for each case are reported in Tables 2 and 3. The figure shows that the Pareto fronts obtained from Case II are more distributed than the Pareto front obtained from Case I. Based on Table 2, the Case I problem obtains the range of structural mass as 115.3216–411.6250 kg while the range of buckling factor obtained is 38.895–1133.1864 Hz. The constraints of critical speed and lift effectiveness are in the ranges of 132.5510–224.1757 m/s and 1.0514–1.1451, respectively. For Case II based on Table 3, the range of structural mass obtained is 125.0137–440.5869 kg while the range of buckling factor obtained is 158.1264–1844.4355 Hz. The constraints, critical speed and lift effectiveness, critical speed of the Pareto front solutions are between 51.8779–219.5524 m/s and 1.0834–1.1639.



(a)



(b)

Figure 9. Pareto frontier and the 10 selected solutions for (a) Case. I. and (b) Case. II.

Table 2. Objective and constraint functions of some selected Pareto solution set from Figure 8a for Case I.

Pareto Front No.	Total Mass [kg.]	1st Buckling [Hz]	Critical Speed [m/s]	Lift Effectiveness [-]	Maximum Transverse Displacement [m.]
1	115.3216	38.895	132.551	1.0514	0.014869
2	121.2212	153.3221	133.3737	1.0783	0.014738
3	133.7867	256.918	137.2478	1.1049	0.012281
4	147.6443	447.1008	143.5185	1.0738	0.0098151
5	235.8701	708.6025	180.0119	1.1208	0.0069166
6	296.3996	923.7469	205.794	1.1257	0.0053827
7	298.355	930.8718	201.5853	1.1323	0.0051402
8	368.1159	932.1128	218.7638	1.1359	0.0047649
9	397.7724	986.4532	224.1757	1.1448	0.0043251
10	411.625	1133.1864	219.5524	1.1451	0.0032751

**Table 3.** Objective and constraint functions of some selected Pareto solution set from Figure 8b for Case. II.

Pareto Front No.	Total Mass [kg.]	1st Buckling [Hz]	Critical Speed [m/s]	Lift Effectiveness [-]	Maximum Transverse Displacement [m.]
1	125.0137	358.1264	51.8779	1.0834	0.013977
2	182.0729	630.0362	84.9946	1.1027	0.0094806
3	186.5354	651.6634	86.7379	1.1084	0.0090102
4	243.907	866.4353	129.7583	1.1275	0.0068166
5	277.4928	1136.3719	114.6718	1.1289	0.0064867
6	288.6587	1280.4411	119.4554	1.1323	0.0062072
7	345.9147	1376.5109	133.3505	1.1452	0.004934
8	355.1918	1421.8814	130.8912	1.1538	0.005063
9	422.4793	1725.0638	139.6456	1.1537	0.0044053
10	440.5869	1844.4355	142.4508	1.1639	0.0043311

For the maximum transverse displacement, constraint minimum and maximum values are 0.0032751 and 0.014869 mm. for Case. I. while they are 0.0043311 and 0.013977 mm. for Case. II.

Figure 10 demonstrates the plots of structural mass versus buckling, lift effectiveness, maximum transverse displacement of the 10 selected solutions for both cases. According to the figure, at the same structural mass, Case II realizes superior buckling and lift effectiveness with slightly better maximum transverse displacement than Case I, whereas Case I exhibited greater critical speed.

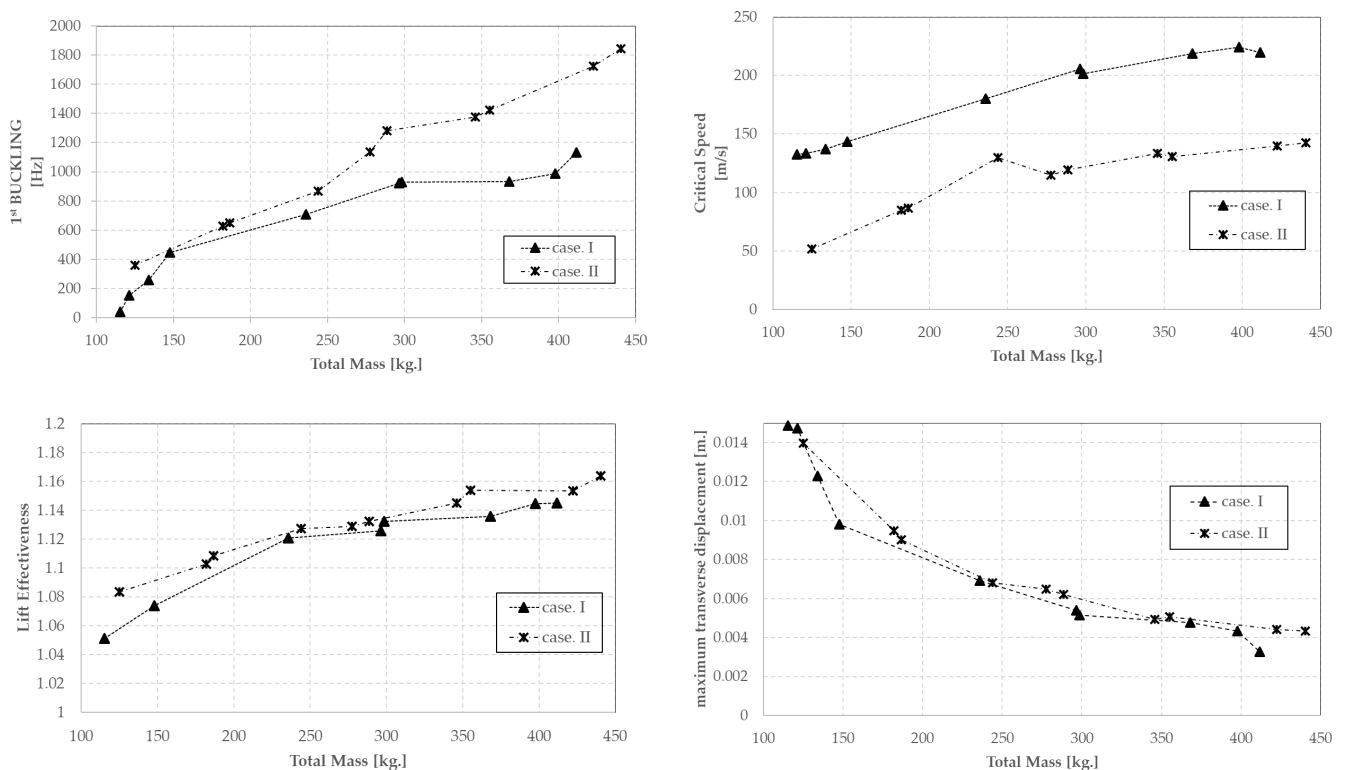


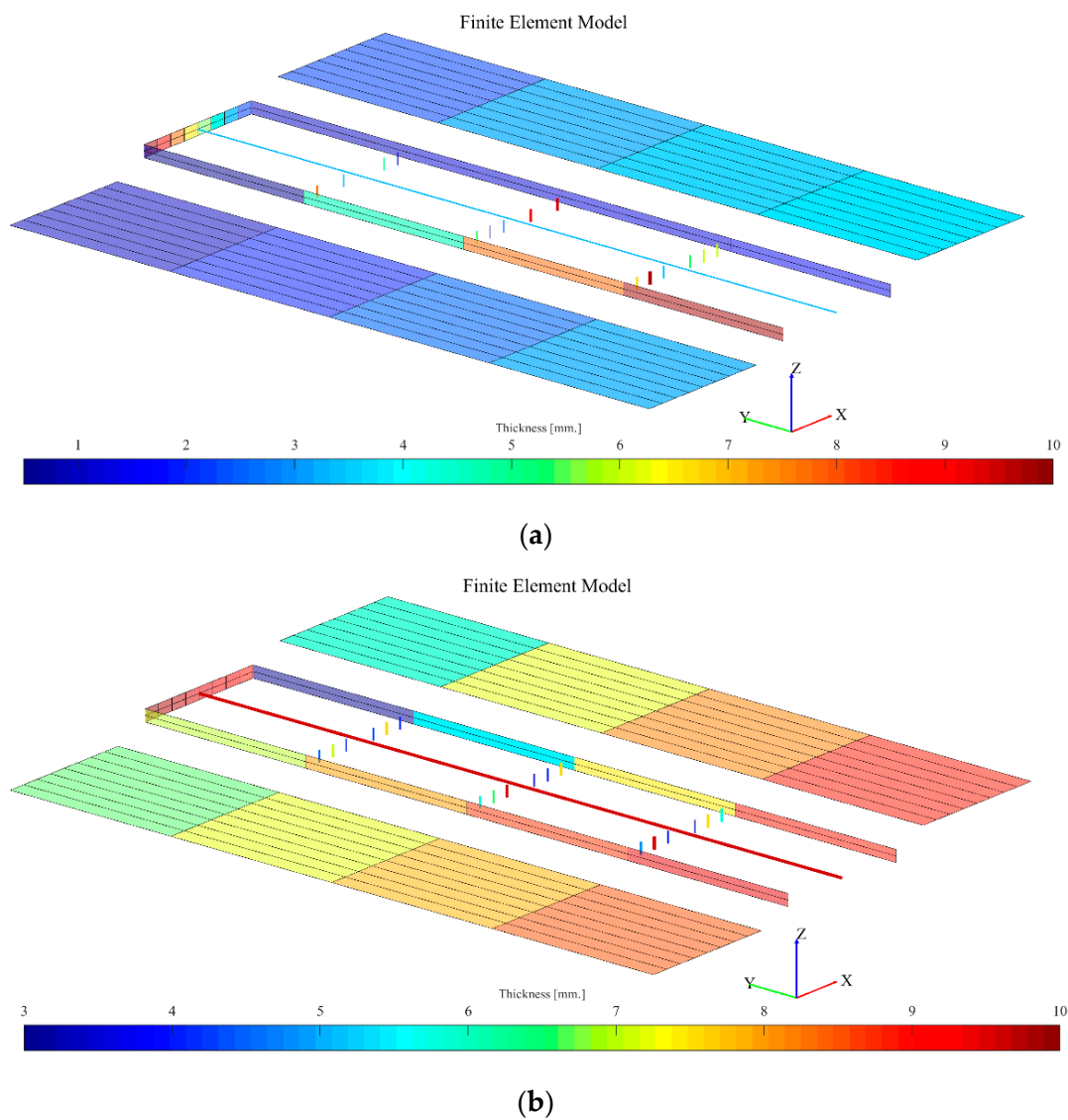
**Figure 10.** Comparison of the buckling, lift effectiveness, maximum transverse displacement, and critical speed in case. I vs. case. II.

With a color bar, Figures 11 and 12 illustrate the topologies and sizes of solutions no. 1 and no. 10 of the 10 selected optimal locations. For both cases, solution no. 1 indicates the points where the least structural mass was obtained, whereas solution no. 10 corresponds to the points where the largest buckling factor was achieved.

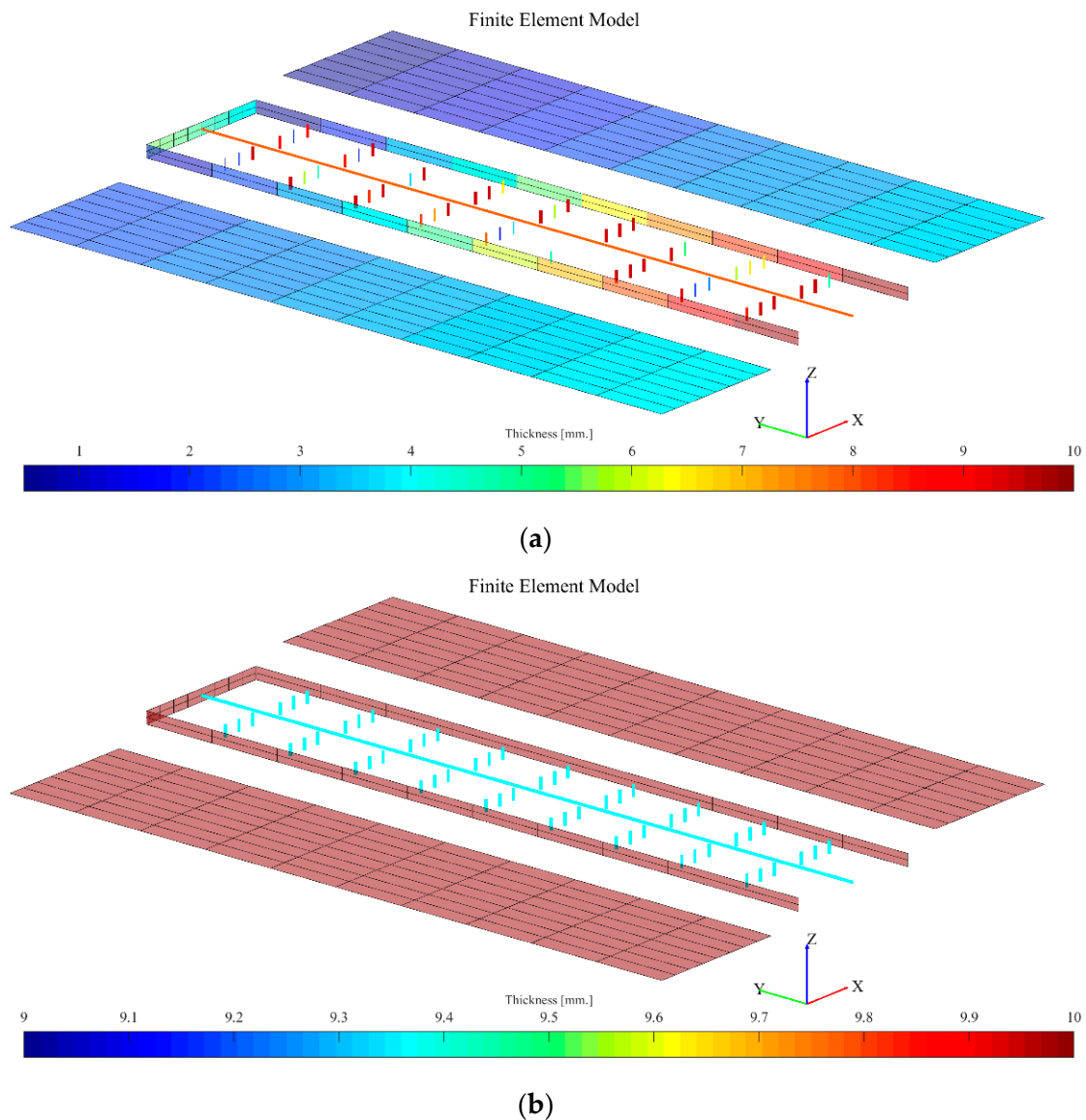
Moreover, for both solutions, it is also evident from Figure 11 that the skeletal rods for no. 10 are larger than that of no. 1, with considerable variation in thicknesses and skeletal rod diameters at the left end (supported) and minor variation at the right end.

Figure 12 depicts the topology altering in Case II against the ground structure of Solution 1, which has the lowest structural mass and buckling factor. The topology of the structure for a solution no. 10, which has the maximum structural mass and buckling factor, is comparable to its ground structure. The variation in thicknesses and skeletal rod diameters are high at the left end (supported) and low at the right end for solution no. 1. For solution no. 10, the thicknesses and skeletal rod diameters have the same size with a larger size than that of no.1.

Overall, it was discovered that the TO issue with better grid resolution acquired a wider range of objective function values when a single MO optimization was performed. Moreover, the higher grid resolution offers the more diverse optimal solutions and topologies of the structure which will be selected through decision-making for the next design steps.



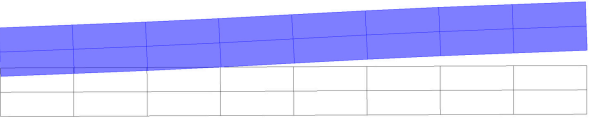
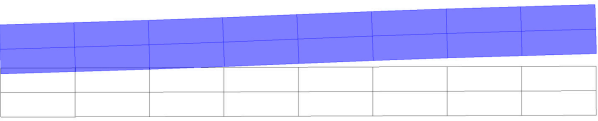
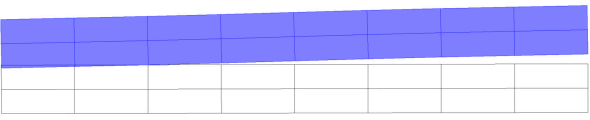
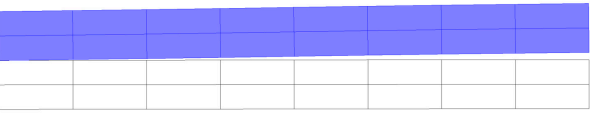
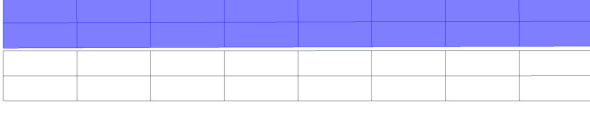
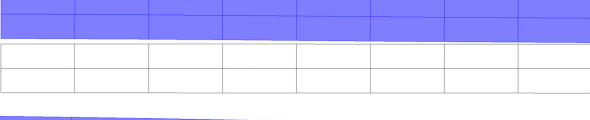
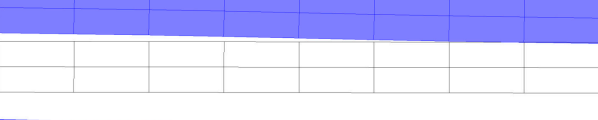
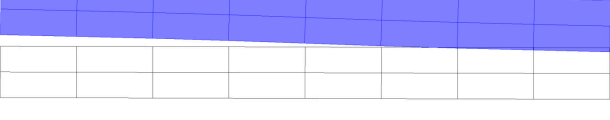
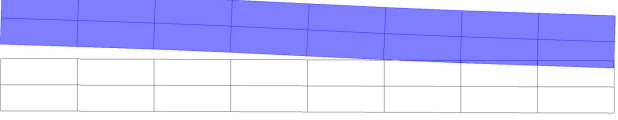
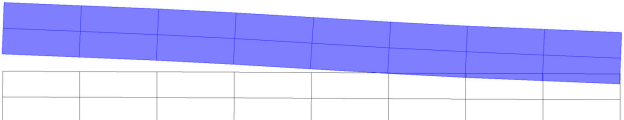
**Figure 11.** Thickness and skeletal rods diameter plot of the selected optimum solutions (a) 1 and (b) 10 Case I with color bar.



**Figure 12.** Thickness and skeletal rods diameter plot of the selected optimum solutions (a) 1 and (b) 10 Case II with color bar.

One optimal design solution is chosen to analyze the wing capability of being morphed. The comparison between jig and cruise shapes of the wing with various values of actuating torque are given in Table 4. It can be seen that when the twisting torque is in a counterclockwise direction, the lift effectiveness becomes higher as higher torque is applied. The wing's front view shows that the cruise shape is bent upward. On the other hand, twisting the beam in a clockwise direction leads to lower wing lift effectiveness while the wing is bent downward from its front view. The maximum range of the lift effectiveness value is  $[0.98322, 1.1957]$ . This implies that the present morphing wing concept has a potential to vary the lift force in the interval of  $[0.98322 L_R, 1.1957 L_R]$  where  $L_R$  is the total lift force on the wing jig shape at cruise speed. That means aircraft lateral/directional motion can be controlled through structural flexibility without using wing ailerons. However, more investigation in various aspects is required before it can lead to a prototype.

**Table 4.** Wing box shapes and lift effectiveness due to actuator torques.

Shape Changing	Lift Effectiveness	Torque (N-m)
		
	1.1957	+1000
	1.1744	+800
	1.1532	+600
	1.1319	+400
	1.1107	+200
	1.0894	0
	1.0682	−200
	1.0470	−400
	1.0257	−600
	1.0045	−800
	0.98322	−1000

**5. Conclusions**

In this work, a new concept of morphing wing structure design is successfully presented based on ground structure topology optimization. Moreover, the effect of the

resolution of the ground structure for the morphing wing on the resulting optimal solutions is investigated. Two multi-objective topology optimization problems are proposed and investigated by employing ground element structures with high- and low-grid resolutions. The design problem has the objectives of weight reduction, difference of lift effectiveness maximization, and buckling factor maximization of an aircraft wing subject to aeroelastic and structural constraints including lift effectiveness, critical speed, and buckling factors. The design variables include aircraft wing structure dimensions and thickness distribution and internal skeletal rod sizing and topology. The MM-IPDE optimizer is used to solve the problems where the optimum results show that the topology optimization problem having higher ground structure resolution gives the higher range of the objective function values. Furthermore, these ground structure designs with high resolution accomplish superior buckling factor and lift effectiveness and slightly better maximum transverse displacement at the same structural mass while the lower ground structure resolution gives the better critical speed at the same structural mass. Moreover, the higher ground structure resolution problem offers more diverse optimal solutions and topologies of the wing structure. In case of testing, the new structure is acceptable for use as a morphing aircraft structure. The result shows that the new structure can change the wing box shape and lift effectiveness upon the applied torques. The new structure concept is said to be acceptable to be used as a morphing aircraft wing.

**Author Contributions:** Conceptualization, K.W., N.P. (Nantiwat Pholdee) and S.B.; methodology, S.W., K.W. and S.B.; setup and designed the numerical experiments, K.W., N.P. (Nantiwat Pholdee) and S.B.; performed the numerical experiments; S.W., S.S. and K.W.; analyzed the data, S.W., N.P. (Natee Panagant) and K.W.; writing—original draft, S.W.; writing—review and editing, S.S., N.P. (Nantiwat Pholdee), N.P. (Natee Panagant), S.K. and S.B. All authors have read and agreed to the published version of the manuscript.

**Funding:** The authors are grateful for the financial support provided by the National Research Council of Thailand (NRCT5-RSA63003-06).

**Institutional Review Board Statement:** Not applicable.

**Informed Consent Statement:** Not applicable.

**Data Availability Statement:** The authors confirm that the data supporting the findings of this study are available within the article.

**Acknowledgments:** The authors are grateful for the financial support provided by the National Research Council of Thailand (NRCT5-RSA63003-06); and the Doctoral Program from Research, Graduate School, Khon Kaen University.

**Conflicts of Interest:** The authors declare no conflict of interest. The funders had no role in the design of the study; in the collection, analyses, or interpretation of data; in the writing of the manuscript, or in the decision to publish the results.

## References

1. Sofla, A.; Meguid, S.; Tan, K.; Yeo, W.K. Design Shape morphing of aircraft wing: Status and challenges. *J. Mater. Des.* **2010**, *31*, 1284–1292. [[CrossRef](#)]
2. Ajaj, R.M.; Parancheerivilakkathil, M.S.; Amoozgar, M.; Friswell, M.I.; Cantwell, W.J. Recent developments in the aeroelasticity of morphing aircraft. *Prog. Aerosp. Sci.* **2021**, *120*, 100682. [[CrossRef](#)]
3. Barbarino, S.O.; Bilgen, R.M.; Ajaj, M.I.; Friswell, D.J. A review of morphing aircraft. *J. Int. Mater. Syst. Struct.* **2011**, *22*, 823–877. [[CrossRef](#)]
4. Love, M.P.; Zink, P.; Wieselmann, P.; Youngren, H. Body freedom flutter of high aspect ratio flying wings. *Struct. Struct. Dyn. Mater. Confer.* **2005**, 1947. [[CrossRef](#)]
5. Ajaj, R.; Friswell, M.; Dettmer, W.; Isikveren, A.; Allegri, G. Conceptual modeling of an adaptive torsion wing structure. *Struct. Confer.* **2011**, *13*, 1883.
6. Ajaj, R.; Friswell, M.; Dettmer, W.; Allegri, G.; Isikveren, A.T. Dynamic modelling and actuation of the adaptive torsion wing. *J. Intell. Mater. Syst. Struct.* **2013**, *24*, 2045–2057. [[CrossRef](#)]
7. Wang, L.; Lui, G.; Qiu, Z. Review: Recent Developments in the Uncertainty-Based Aero-Structural Design Optimization for Aerospace Vehicles. *J. Harbin Inst. Tech.* **2018**, *25*, 1–15.

8. Burdette, D.A.; Martins, J.R. Design of a transonic wing with an adaptive morphing trailing edge via aerostructural optimization. *Aerosp. Sci. Technol.* **2018**, *81*, 192–203. [[CrossRef](#)]
9. Molinari, G.; Quack, M.; Arrieta, A.F.; Morari, M.; Ermanni, P. Realization and structural testing of a compliant adaptable wing. *Smart Mater. Struct.* **2015**, *24*, 105027. [[CrossRef](#)]
10. Henry, C.; Molinari, G.; Rivas-Padilla, J.R.; Arrieta, A.F. Smart morphing wing: Optimization of distributed piezoelectric actuation. *AIAA J.* **2019**, *57*, 2384–2393. [[CrossRef](#)]
11. Grihon, S.; Krog, L.; Tucker, A.; Hertel, K. A380 weight savings using numerical structural optimization. In Proceedings of the 20th AAAF Colloquium on Material for Aerospace Applications, Paris, France, 24–26 November 2004; pp. 763–766.
12. Krog, L.; Tucker, A.; Kemp, M.; Boyd, R. Topology optimization of aircraft wing box ribs. In Proceedings of the 10th AIAA/ISSMO Multidisciplinary Analysis and Optimization Conference, New York, NY, USA, 30 August–1 September 2004.
13. Saitou, K.; Izui, K.; Nishiwaki, S.; Papalambros, P. A survey of structural optimization in mechanical product development. *Trans. ASME* **2005**, *5*, 214–226. [[CrossRef](#)]
14. Rothwell, A. Multi-level optimization of aircraft shell structures. *Thin-Walled Struct.* **1991**, *11*, 85–103. [[CrossRef](#)]
15. Lencus, A.; Querin, O.M.; Steven, G.P.; Xie, Y.M. Aircraft wing design automation with ESO and GESO. *Int. J. Veh. Des.* **2001**, *28*, 98–111. [[CrossRef](#)]
16. Harzen, L.U.; Peter, H. Multilevel optimization in aircraft structural design evaluation. *Comput. Struct.* **2008**, *86*, 104–118.
17. Slesongsom, S.; Bureerat, S. New conceptual design of aeroelastic wing structures by multiobjective optimization. *Eng. Optim.* **2013**, *45*, 107–122. [[CrossRef](#)]
18. Bendsoe, M.; Sigmund, O. *Topology Optimization*; Springer: Berlin/Heidelberg, Germany, 2003.
19. Saggere, L.; Kota, S. Static shape control of smart structures using compliant mechanisms. *AIAA J.* **1999**, *37*, 572–578. [[CrossRef](#)]
20. Slesongsom, S.; Bureerat, S. Aircraft morphing wing design by using partial topology optimization. *Struct. Multidiscip. Optim.* **2013**, *48*, 1109–1128. [[CrossRef](#)]
21. Slesongsom, S.; Bureerat, S. Morphing Wing Structural Optimization Using Opposite-Based Population-Based Incremental Learning and Multigrid Ground Elements. *Mathemat. Probl. Eng.* **2015**, *2015*, 730626. [[CrossRef](#)]
22. Meng, L.; Zhang, W.; Quan, D.; Shi, G.; Tang, L.; Hou, Y.; Breitkopf, P.; Zhu, J.; Gao, T. From topology optimization design to additive manufacturing: Today's success and tomorrow's roadmap. *Arch. Comput. Methods Eng.* **2020**, *27*, 805–830. [[CrossRef](#)]
23. Stanford, B.; Dunning, P.D. Optimal Topology of Aircraft Rib and Spar Structures under Aeroelastic Loads. *J. Aircr.* **2015**, *52*, 1298–1311. [[CrossRef](#)]
24. Stanford, B. Aeroelastic Wing box stiffener topology optimization. *J. Aircr.* **2018**, *55*, 1244–1251. [[CrossRef](#)]
25. Stanford, B.; Beran, B.; Bhatia, M. Aeroelastic Topology Optimization of Blade-Stiffened Panels. *J. Aircr.* **2014**, *51*, 938–944. [[CrossRef](#)]
26. Maute, K.; Allen, M. Conceptual design of aeroelastic structures by topology optimization. *Struct. Multidiscip. Optim.* **2004**, *27*, 27–42. [[CrossRef](#)]
27. Townsend, S.; Kim, H. A level set topology optimization method for the buckling of shell structures. *Struct. Multidiscip. Optim.* **2019**, *60*, 1783–1800. [[CrossRef](#)]
28. Yang, W.; Yue, Z.; Li, L.; Wang, P. Aircraft wing structural design optimization based on automated finite element modelling and ground structure approach. *Eng. Optim.* **2016**, *48*, 94–114. [[CrossRef](#)]
29. Fasel, U.; Keidel, D.; Baumann, L.; Cavolina, G.; Eichenhofer, M.; Ermanni, P. Composite additive manufacturing of morphing aerospace structures. *Manuf. Lett.* **2020**, *23*, 85–88. [[CrossRef](#)]
30. Song, L.; Gao, T.; Tang, L.; Du, X.; Zhu, J.; Lin, Y.; Shi, G.; Liu, H.; Zhou, G.; Zhang, W. An all-movable rudder designed by thermo-elastic topology optimization and manufactured by additive manufacturing. *Comput. Struct.* **2021**, *243*, 106405. [[CrossRef](#)]
31. Slesongsom, S.; Yooyen, S.; Prapamonthon, P.; Bureerat, S. Reliability-based Design Optimization of Classical Wing Aeroelasticity. *IOP Conf. Ser. Mater. Sci. Eng.* **2020**, *886*, 012015. [[CrossRef](#)]
32. Wansaseub, K.; Slesongsom, S.; Panagant, N.; Pholdee, N.; Bureerat, S. Surrogate-Assisted Reliability Optimisation of an Aircraft Wing with Static and Dynamic Aeroelastic Constraints. *Int. J. Aeronaut. Space* **2020**, *21*, 723–732. [[CrossRef](#)]
33. Winyangkul, S.; Slesongsom, S.; Bureerat, S. Reliability-Based Design of an Aircraft Wing Using a Fuzzy-Based Metaheuristic. *Appl. Sci.* **2021**, *11*, 6463. [[CrossRef](#)]
34. Wansaseub, K.; Pholdee, N.; Panagant, N.; Bureerat, S. Multiobjective meta-heuristic with iterative parameter distribution estimation for aeroelastic design of an aircraft wing. *J. Eng. Comput.* **2020**, *45*, 1–19. [[CrossRef](#)]
35. Guo, S.; Li, D.; Liu, Y. Multi-objective optimization of a composite wing subject to strength and aeroelastic constraints. *Part G J. Aerosp. Eng.* **2012**, *226*, 1095–1106. [[CrossRef](#)]